3.3 Strongly Correlated Quantum Systems

Numerical Studies on Superconductivity of Bilaye Cuprates and Mott Insulating States of Kitaev Materials

Youhei YAMAJI
Research Center for Materials Nanoarchitectonics, National Institute for Materials Science
Namiki, Tsukuba-shi, Ibaraki 305-0044

We have studied properties of two families of typical correlated electron systems, cuprate high-temperature superconductors and quantum-spin-liquid candidates, by using many-variable variational Monte Carlo methods [1]. As detailed below, we found that adjacent CuO_2 layer does not improve stability of the d-wave superconductivity in Hubbard-type hamiltonians [2], which are effective hamiltonians for the bilayer cuprates. We also studied propertie of an *ab initio* hamiltonian of a Kitaev material, Na_2IrO_3 [3, 4].

We studied the superconducting correlation function at long distance, P_d, for the bilayer t-t' Hubbard model around $U/t = 10$ and $t'/t \sim -0.3$. When we change a hole concentration, we found that the maximum P_d is quantitatively similar for the single-layer and bilayer t-t' Hubbard models [2]. From the momentum distribution functions, $n_{\boldsymbol{k}}$, we estimated the size of the superconducting gap Δ. Then, the effective attractive interaction, V_d, can be inferred by $V_d = \Delta/\sqrt{P_d}$. For both of the single-layer and bilayer systems, we obtain $V_d \sim 1.7t$. The variety of the optimal critical temperatures of cuprates may originate from the screening from apical oxygen and, thus, mainly from the Hubbard U [5, 6].

We also studied the properties of Na_2IrO_3 beyond low-energy spin degrees of freedom. First, we clarified the ground state of the *ab initio* t_{2g} hamiltonian [3]. We confirmed that the ground state shows the zigzag magnetic order, and found that the the amplitude of the Mott gap is 750 meV, which is larger than 340 meV reported by combining the optical conductivity and photoemission spectroscopy [7]. The discrepancy originates from the Mott-Andern nature of the experimentally observed samples of Na_2IrO_3 due to disorders, where the Mott gap is filled by in-gap localized states. When the principle energy scales, the on-site (off-site) Coulomb repulsion U (V_{ij}) and spin-orbit coupling $\zeta_{\rm so}$, are deviated from the *ab initio* values, the first order phase transitions from the zigzag state to ferromagnetic and charge ordered states are found.

References

[1] T. Misawa, *et al.*: Comput. Phys. Commun. **235**, 447 (2019).

[2] A. Iwano and Y. Yamaji: J. Phys. Soc. Jpn. **91**, 094702 (2022).

[3] Y. Yamaji, *et al.*: Phys. Rev. Lett. **113**, 107201 (2014).

[4] C. Xu and Y. Yamaji: in preparation.

[5] J.-B. Morée, *et al.*: Phys. Rev. B **106**, 235150 (2022).

[6] M. T. Schmid, *et al.*: arXiv:2303.06672.

[7] R. Comin, *et al.*: Phys. Rev. Lett. **109**, 266406 (2012).

Theoretical study of strongly-correlated topological phenomena by exploiting first-principles calculations and machine learning

Yukitoshi MOTOME

Department of Applied Physics,

The University of Tokyo, Bunkyo, Tokyo 113-8656

We have theoretically studied a variety of intriguing topological phenomena in strongly-correlated electron systems by using numerical methods including first-principles calculations and machine learning (project numbers: 2022-Ca-0013 and 2022-Cb-0013). During the last fiscal year, we have achieved substantial progress on the following topics. We summarize the main results below.

(i) *Development of new theoretical methods*: We developed a new framework to solve "inverse problem", namely to construct a proper Hamiltonian which exhibits desired physical properties, by using automatic differentiation [1]. We also proposed a new scheme for physical reservoir computing by exploiting frustrated magnets, which is useful to realize efficient parallel computing in both space and time [2,3].

(ii) *Topological properties of thin films of Weyl semimetals*: Studying the structural, electronic, and magnetic properties of atomically thin films of Co-based shandite by first-principles calculations, we clarified the changes of magnetism and band topology with respect to the number of Co kagome layers and the surface termination, which will be useful for future experimental fabrication [4].

(iii) *Topological spin crystals as spin moire*: Extending the research in last year, we clarified the effect of phase shift on skyrmion and hedgehog crystals and elucidated the topological phase diagrams [5]. We also showed that hedgehog crystals can be stabilized in centrosymmetric cubic lattices by itinerant frustration mechanism [6]. In addition, we developed a new exact method to solve thermodynamics of effective infinite-range interaction models [7], and by applying it we unveiled hidden topological transitions associated with pair creation and annihilation of emergent magnetic monopoles [8].

(iv) *Kitaev quantum spin liquids*: By using the pseudo-fermion functional renormalization group (PFFRG) method, we clarified the feasibility of Kitaev quantum spin liquids in ultracold polar molecules [9], a complete phase diagram for the Kitaev-Heisenberg model with arbitrary spin length S [10], and the phase diagram for the S=1/2 Kitaev-Heisenberg

model on a three-dimensional hyperhoneycomb lattice [11]. We also unveiled several exotic phases, including multiple-q chiral phases and chiral spin liquid, in competing region between spin nematics and spin liuqids in the S=1 Kitaev model with bilinear-biquadratic interactions by using the SU(3) formalism [12]. We elucidated linear and nonlinear thermal transport in the presence of both uniform and staggered magnetic fields [13]. In addition, we clarified that the dynamical spin transport induced by an AC magnetic field applied to an edge of the system is useful for the identification of fractional excitations in the Kitaev quantum spin liquids [14]. Furthermore, we found a phase transition in the quantum spin liquid phase under a magnetic field in α-$RuCl_3$ in collaboration with experimentalists [15]. We also wrote a review article (in Japanese) [16] in a special issue for “New Developments on the Physics of Kitaev Spin Liquids” edited by the author and coworkers [17].

References

[1] K. Inui and Y. Motome, Commun. Phys. **6**, 37 (2023).

[2] K. Kobayashi and Y. Motome, preprint (arXiv:2302.14496).

[3] 特願 2023-025883「情報処理システム、情報処理方法およびプログラム」求 幸年、小林海翔（2023 年 2 月 22 日出願）

[4] K. Nakazawa, Y. Kato, and Y. Motome, preprint (arXiv:2212.09026).

[5] K. Shimizu, S. Okumura, Y. Kato, and Y. Motome, Phys. Rev. B **105**, 224405 (2022).

[6] S. Okumura, S. Hayami, Y. Kato, and Y. Motome, J. Phys. Soc. Jpn. **91**, 093702 (2022).

[7] Y. Kato and Y. Motome, Phys. Rev. B **105**, 174413 (2022).

[8] Y. Kato and Y. Motome, Phys. Rev. B **107**, 094437 (2023).

[9] K. Fukui, Y. Kato, J. Nasu, and Y. Motome, Phys. Rev. B **106**, 014419 (2022).

[10] K. Fukui, Y. Kato, J. Nasu, and Y. Motome, Phys. Rev. B **106**, 174416 (2022).

[11] K. Fukui, Y. Kato, and Y. Motome, preprint (arXiv:2303.09156).

[12] R. Pohle, N. Shannon, and Y. Motome, Phys. Rev. B **107**, L140403 (2023).

[13] K. Nakazawa, Y. Kato, and Y. Motome, Phys. Rev. B **105**, 165152 (2022).

[14] T. Misawa, J. Nasu, and Y. Motome, preprint (arXiv:2304.00528).

[15] S. Suetsugu, Y. Ukai, M. Shimomura, M. Kamimura, T. Asaba, Y. Kasahara, N. Kurita, H. Tanaka, T. Shibauchi, J. Nasu, Y. Motome, and Y. Matsuda, J. Phys. Soc. Jpn. **91**, 124703 (2022).

[16] 張 成燻、求 幸年：固体物理 **57**, 757 (2022).

[17] 固体物理特集号 **57**, 613-784 (2022), "キタエフスピン液体の新展開" (編集委員：芝内孝禎・遠山貴巳・求 幸年)

Theoretical study on elementaly excitations and optical control of topological phases in the spin-charge coupled magnets

Rintaro ETO and Masahito MOCHIZUKI
Department of Applied Physics, Waseda University
Okubo, Shinjuku-ku, Tokyo 169-8555

We have theoretically studied elementaly excitations and photoinduced topological phases in the Kondo-lattice magnets with couplings between spin and charge degrees of freedom (project ID: 2022-Ca-0012, 2022-Cb-0014). Results of these projects are listed below.

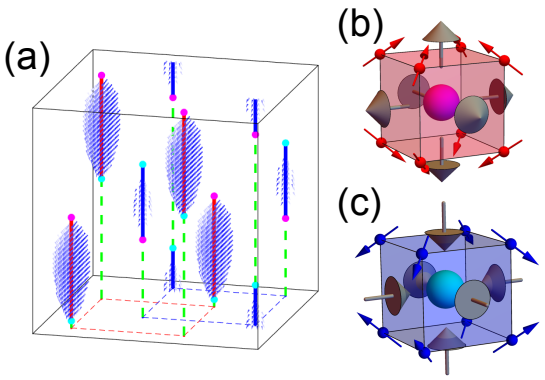

Figure 1: (a) Schematic of the quadruple-Q hedgehog lattice. Magenta and cyan balls represent hedgehogs and antihedgehogs, respectively. Red and blue dashed lines represent the Dirac strings A (vortex type) and B (antivortex type), respectively. (b),(c) Enlargements of the (b) hedgehog and (c) antihedgehog. Gray arrows denote local emergent magnetic fields.

(i) *Spin-wave excitations in the quadruple-Q magnetic hedgehog lattices in 3D chiral magnets*: We have theoretically studied the spin-wave modes of the quadruple-Q magnetic hedgehog lattices in 3D chiral magnets [Fig. 1(a)] [1]. First, we constructed a microscopic Kondo-lattice model on the 3D cubic lattice, which hosts the quadruple-Q hedgehog lattice spin textures as the ground state. In this model, interplay of the second- and fourth-order spin-spin interactions mediated by nested Fermi surfaces is a key to stabilizing the hedgehog lattice spin textures. The hedgehog lattice spin textures in this model have two types of Dirac strings connecting a hedgehog [Fig. 1(b)] and an antihedgehog [Fig. 1(c)], the vortex-type strings A and the antivortex-type strings B. Using this model, we studied the spin-wave excitations of the hedgehog lattice spin textures under an external magnetic field ($\parallel$ [001]) by using large-scale adiabatic spin-dynamics simulations based on the kernel polynomial method. By calculating the microwave absorption spectra for microwave polarization parallel to the Dirac strings (i.e. $\parallel$ [001]), we found three spin-wave nmodes, which are named L1, L2, and L3, in order from the lowest to highest frequency. These modes are spatially localized at the Dirac strings and are associated with translational motion of the Dirac strings. In particular, the disappearance of L2 mode, which is localized at the strings B, is observed simultaneously with the field-induced hedgehog-antihedgehog pair annihilation at the strings B.

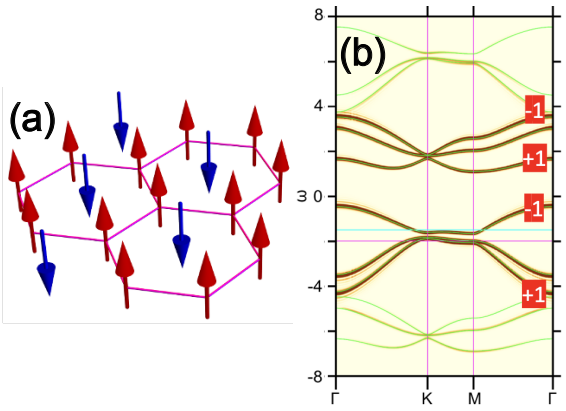

Figure 2: (a) Schematic of the three-sublattice ferrimagnetic order. Majority spins form a honeycomb network. (b) Single-particle spectrum of a Floquet Chern insulator state. Green lines represent the Floquet states. Numbers are the Chern numbers of the corresponding bands.

(ii) *Floquet topological phases in the Dirac half-metallic ferrimagnet*: We have theoretically investigated photoinduced topological phases in the Dirac half-metallic state in the spin-charge coupled Kondo-lattice magnets [2]. We here considered the three-sublattice ferrimagnetic order on the 2D triangular lattice which appears spontaneously when the conduction electron filling is 1/3 [Fig. 2(a)]. We analyzed this model using the Floquet theory and found two types of Floquet Chern insulator (FCI) states with gapped spin-polarized Dirac bands. One is associated with the gap opening at K point [Fig. 2(b)], whereas the other originates from the gap closing and reopening at M point. The appearance of the former FCI state was also confirmed in our analysis of the periodic Anderson model, from which the Kondo-lattice model is derived via the perturbational calculation. Both of these FCI states are induced not by the first-order but by the higher-order terms in the high-frequency expansion, and are distinct from conventional ones induced by the first-order terms associated with the original sublattice degrees of freedom of the honeycomb lattice. This work will extend the scope of Floquet engineering to magnetic materials with sublattice degrees of freedom of magnetic origin.

References

[1] R. Eto and M. Mochizuki, in preparation.

[2] R. Eto and M. Mochizuki, in preparation.

Studies on superconductivity in trestle-type lattices

KAZUHIKO KUROKI
Department of Physics, Osaka University
1-1 Machikaneyama, Toyonaka, Osaka, 560-0043, Japan

INTRODUCTION

Most cuprate superconductors possess CuO_2 planes, which are considered to play the main role in the occurrence of superconductivity. One exception is $(Sr,Ca)_{14}Cu_{24}O_{41}$[1], which consists of two-leg ladder and chain structures. Yet another possible example is $Pr_2Ba_4Cu_7O_{15-\delta}$[2]. This material is constructed from alternating stacking of $PrBa_2Cu_3O_7$ and $PrBa_2Cu_4O_8$, and does have CuO_2 planes, but they are considered to be insulating. There have been suggestions that the double-chain structure in $PrBa_2Cu_4O_8$ is responsible for the superconductivity, and some theoretical studies support this possibility[3–5]. Quite recently, there has been stronger evidences that the double-chain structure is responsible for the occurrence of superconductivity[6].

FLEX STUDIES ON THE HUBBARD MODEL ON A TRESTLE-TYPE LATTICE

The double-chain structure can be modeled by a Hubbard model on a trestle-type lattice, with intra-chain hopping t_2 and interchain hopping t_1. This model can further be considered as a single band one-dimensional system with nearest (t_1) and next nearest (t_2) neighbor hoppings. We theoretically studied this model using the fluctuation exchange (FLEX) approximation. We have varied t_2/t_1 as well as the band filling, and obtained the eigenvalue of the Eliashberg equation at a fixed temperature, which measures tendency towards superconductivity. Depending on the parameter values, there can be either two or four Fermi points because the band structure has a double-well shape. The case where there are four Fermi points resembles the situation for the two-leg ladder systems. We find that the eigenvalue of the Eliashberg equation becomes the largest when the band intersects the Fermi level at two Fermi points and also barely touches the Fermi level at two other points. This is in fact reminiscent of the situation where one of the bands is incipient in the two-leg ladder system[7]. Studies applying other many-body methods to this model are underway in order to verify these FLEX results.

FIRST-PRINCIPLES MODEL CONSTRUCTION OF $PR_2BA_4CU_7O_{15-\delta}$

In order to obtain a realistic model of $Pr_2Ba_4Cu_7O_{15-\delta}$, we have performed first principles band calculation of this material using VASP, and obtained a tightbinding model for the double-chain structure through wannierization. A relatively large t_1/t_2 ratio is obtained, consistent with previous studies[3–5]. Many-body study of this realistic model is now underway. An important point we are focusing on is (i) the band filling of the double-chain structure as a function of oxygen deficiency δ and (ii) the origin of the relatively large t_1/t_2, which is essential in obtaining the tendency toward superconductivity.

[1] M. Uehara *et al.*, J. Phys. Soc. Jpn. **65**, 2764 (1996).
[2] M. Matsukawa *et al.*, Physica C **411**, 1011 (2004).
[3] K. Sano, Y.Ono, and Y. Yamada, J. Phys. Soc. Jpn. **74**, 2885 (2005).
[4] T. Nakano and K. Kuroki, Phys. Rev. B **76**, 014515 (2007).
[5] T. Habaguchi *et al.*, J. Phys. Soc. Jpn. **80**, 024708 (2011).
[6] S. Nishioka *et al.*, Appl. Phys. Exp. **15**, 023001 (2022).
[7] K. Matsumoto, D. Ogura, and K. Kuroki, Phys. Rev. B **97**, 014516 (2018).

First-principles calculations of dynamical susceptibilities for strongly correlated materials

Hiroshi SHINAOKA

Department of Physics, Saitama University, Saitama 338-8570

This report details our recent computational investigation of $SrRu_2O_6$, a material around the boundary between covalent and Mott insulators. Our study aimed to compare the results with those of inelastic scattering experiments, and for this purpose, we employed the density functional theory plus the dynamical mean-field theory (DFT+DMFT) approach. We used DCore [1] and ALPS/CT-HYB [2] for DFT+DMFT calculations. The codes are parallelized by MPI. We constructed the tight-binding model using Wien2k.

We successfully created a phase diagram as a function of temperature. Notably, we observed an antiferromagnetic phase at low temperatures consistent with experimental findings. Figure 1 plots the temperature dependence of the magnetic moment.

Currently, we are calculating the dynamic susceptibility in the low-temperature phase by solving the Bethe-Salpeter equation. We expect to release our results as a preprint [3].

It is important to acknowledge that this research has been conducted as a collaboration between Prof. Atsushi Hariki at Osaka City University and the group of Jan Kuneš at TU Wien.

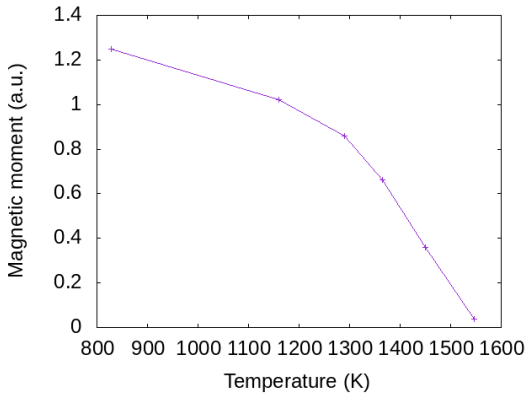

Fig. 1: Temperature dependence of magnetic moment

References

[1] H. Shinaoka, J. Otsuki, M. Kawamura, N. Takemori, K. Yoshimi, SciPost Phys. 10, 117 (2021).

[2] H. Shinaoka, E. Gull, P. Werner, Comput. Phys. Commun. 215, 128 (2017).

[3] Diana Csontosová, H. Shinaoka, A. Hariki, and J. Kuneš, in preparation.

Nonlocal correlation effects in a Hund Ferromagnet

Yusuke NOMURA

Department of Applied Physics and Physico-Informatics, Keio University,

3-14-1 Hiyoshi, Kohoku-ku, Yokohama, 223-8522, Japan

Understanding electron correlation effects beyond Fermi liquid theory is a fundamental problem in condensed matter physics, since various intriguing phenomena such as superconductivity and magnetism emerge from pseudogap and strange-metal states.

A well-known example is the pseudogap behavior observed in doped cuprates, where strong nonlocal antiferromagnetic fluctuations are believed to play an important role. This phenomenon has been intensively studied by the cluster extension of the dynamical mean-field theory.

However, nonlocal correlation effects in multi-orbital systems remain largely elusive. In particular, the influence of ferromagnetic fluctuations in the strong-coupling regime is still poorly understood compared to the antiferromagnetic case.

Such a strong-coupling ferromagnetic regime is expected in the multiorbital Hubbard model. Therefore, we study the two-orbital Hubbard model on the two-dimensional square lattice using cellular dynamical mean-field theory. Although the cluster extension in multiorbital systems is computationally expensive, we have managed to accomplish the calculations thanks to the efficient continuous-time quantum Monte Carlo methods developed in Refs. [1-4].

We find that the Fermi surface expands even above the Curie temperature as if the spin polarization occurred, contrary to a naïve view that the Fermi surface should recover non-spin-polarized behavior. Behind this phenomenon, effective “Hund’s physics” works in momentum space; ferromagnetic spin correlations induce effective Hund’s coupling in momentum space, leading to a large modulation of the momentum space occupancy. The reconstruction of the Fermi surface differs from the antiferromagnetic case, where it creates hot and cold spots in the Fermi surface. Our finding will give a deeper insight into the physics of Hund’s ferromagnets above the Curie temperature.

References

[1] Y. Nomura, S. Sakai, and R. Arita, Phys. Rev. B **89**, 195146 (2014)

[2] H. Shinaoka, Y. Nomura et al., Phys. Rev. B **92**, 195126 (2015)

[3] Y. Nomura, S. Sakai, and R. Arita, Phys. Rev. B **91**, 235107 (2015)

[4] H. Shinaoka, Y. Nomura and E. Gull,

Comput. Phys. Commun. **252**, 106826 (2020)

[5] Y. Nomura, S. Sakai, and R. Arita, Phys. Rev. Lett. **128**, 206401 (2022)

Transient absorption spectrum in photo-excited one-dimensional Mott insulators

Takami TOHYAMA
Department of Applied Physics, Tokyo University of Science, Tokyo 125-8585

The elucidation of nonequilibrium states in strongly correlated systems is of great interest since it promises to open a door to the emergence of novel quantum phases. One of the most significant challenges is how to preserve nonequilibrium states, such as the Floquet states, from thermalization, for which the realization of many-body localization may hold the key. Also, the nonequilibrium-induced insulator-to-metal transition studied extensively in the one-dimensional (1D) Mott insulator is a fundamental issue associated with competition between itinerancy and localization of charge degrees of freedom. Similarly, non-absorbable terahertz photons with strong intensity may induce a metallic state via quantum tunneling. Until now it has been commonly accepted that the breakdown of the Mott insulators via electric pulses leads to metallic states. However, we raise question about the validity of this understanding.

To answer this question, in this project we focus on the possibility of the emergence of novel quantum phases such as glass phases with intermediate properties between itinerancy and many-body localization. We investigate pulse-excited states of the half-filled 1D extended Hubbard model using the time-dependent density-matrix renormalization group (tDMRG). Our tDMRG makes use of the Legendre polynomial for the calculation of time-evolution operator. We use two target states at a given time t and $t + \Delta t$ to construct a basis set that can express wavefunctions in the time-dependent Hilbert space. With the two-target tDMRG procedure, we can calculate time-dependent physical quantities with high accuracy even when the Hamiltonian varies rapidly with time.

From our tDMRG simulations, we propose a Mott transition to glassy states induced by mono- and half-cycle terahertz pulses **??**. If we excite the Mott insulating state via photon absorption, we obtain metallic states with large Drude weight. In contrast, we find that strong electric fields inducing the Zener breakdown strongly suppress the Drude weight even in the presence of a large number of carriers. We consider that the Hilbert-space fragmentation due to high fields leads to glassy dynamics as seen in fracton systems. The glassy state is accompanied by electric polarization that breaks inversion symmetry **??**. We also demonstrate a steady electric current induced by an ultrashort subcycle pulse. This is due to an Aharonov-Bohm flux introduced through the phase of an electric field. Consequently, time-reversal symmetry is broken. Both symmetry breakings can be monitored by second harmonic generation. These findings propose a new methodology for designing the symmetries of electronic states and open up a new field of subcycle-pulse engineering.

References

[1] K. Shinjo, S. Sota, and T. Tohyama: Phys. Rev. Res **4** (2022) L032019.

[2] K. Shinjo, S. Sota, S. Yunoki, and T. Tohyama: arVix:2211.08694.

Research of Three-Channel Kondo Effect Emerging from Holmium Ions

Takashi HOTTA
Department of Physics, Tokyo Metropolitan University
1-1 Minami-Osawa, Hachioji, Tokyo 192-0397

In 2021, we have discovered the three-channel Kondo effect emerging from Ho ions [1]. Here we briefly report the subsequent development of the research, in particular, the magnitude of the effective impurity spin of the three-channel Kondo effect.

First we explain the model Hamiltonian. For the construction of the model, we define one f-electron state by the eigenstate of spin-orbit and crystalline electric field (CEF) potential terms. We obtain Γ_7 doublet and Γ_8 quartet from $j = 5/2$ sextet whereas we find Γ_6 doublet, Γ_7 doublet, and Γ_8 quartet from $j = 7/2$ octet under the cubic CEF potential. Then, we include the Γ_7 and Γ_8 conduction electron bands. Here we consider only the hybridization between the conduction and $j = 7/2$ electrons. The model Hamiltonian is given by

$$\begin{aligned} H &= \sum_{\boldsymbol{k},\mu,\tau} \varepsilon_{\boldsymbol{k}} c^\dagger_{\boldsymbol{k}\mu\tau} c_{\boldsymbol{k}\mu\tau} + \sum_{\boldsymbol{k},\mu,\tau} V(c^\dagger_{\boldsymbol{k}\mu\tau} f_{b\mu\tau} + \text{h.c.}) \\ &+ nE_f + \sum_{j,\mu,\tau} (\lambda_j + B_{j,\mu}) f^\dagger_{j\mu\tau} f_{j\mu\tau} \\ &+ \sum_{j_1\sim j_4} \sum_{\mu_1\sim\mu_4} \sum_{\tau_1\sim\tau_4} I^{j_1 j_2, j_3 j_4}_{\mu_1\tau_1\mu_2\tau_2,\mu_3\tau_3\mu_4\tau_4} \\ &\times f^\dagger_{j_1\mu_1\tau_1} f^\dagger_{j_2\mu_2\tau_2} f_{j_3\mu_3\tau_3} f_{j_4\mu_4\tau_4}, \end{aligned} \tag{1}$$

where $\varepsilon_{\boldsymbol{k}}$ is the dispersion of conduction electron with wave vector $\boldsymbol{k}$, $c_{\boldsymbol{k}\mu\tau}$ is the annihilation operator of a conduction electron, $f_{j\mu\tau}$ is the annihilation operator of a localized f electron in the bases of (j, μ, τ), j is the total angular momentum, $j = 5/2$ and $7/2$ are denoted by "a" and "b", respectively, μ distinguishes the cubic irreducible representation, Γ_8 states are distinguished by $\mu = \alpha$ and β, while the Γ_7 and Γ_6 states are labeled by $\mu = \gamma$ and δ, respectively, τ denotes the pseudo-spin, which distinguishes the degeneracy concerning the time-reversal symmetry, V denotes the hybridization between f electron in the μ orbital and conduction electron of the μ band, n is the local f-electron number at an impurity site, and E_f is the f-electron level to control n.

As for the spin-orbit term, we obtain $\lambda_a = -2\lambda$ and $\lambda_b = (3/2)\lambda$, where λ is the spin-orbit coupling of f electron and we set $\lambda = 0.265$ eV for the Ho ions. Concerning the CEF potential term for $j = 5/2$, we obtain $B_{a,\alpha} = B_{a,\beta} = 1320B^0_4/7$ and $B_{a,\gamma} = -2640B^0_4/7$, where B^0_4 denotes the fourth-order CEF parameter for the angular momentum $\ell = 3$. For $j = 7/2$, we obtain $B_{b,\alpha} = B_{b,\beta} = 360B^0_4/7 + 2880B^0_6$, $B_{b,\gamma} = -3240B^0_4/7 - 2160B^0_6$, and $B_{b,\delta} = 360B^0_4 - 3600B^0_6/7$. In the following calculations, we use the parametrization as $B^0_4 = Wx/15$ and $B^0_6 = W(1 - |x|)/180$ for $\ell = 3$, where x specifies the CEF scheme for the $O_{\rm h}$ point group, while W determines the energy scale of the CEF potentials. In this work, we set $W = 10^{-3}$ eV and treat x as the parameter to control the CEF ground state.

For the Coulomb interaction terms, we do not show the explicit forms of I here, but they are expressed by the four Slater-Condon parameters, F^0, F^2, F^4, and F^6. These values should be determined from experimental results, but here we simply set the ratio as $F^0/10 = F^2/5 = F^4/3 = F^6 = U$, where U indicates the Hund's rule interaction among the

f orbitals. In this work, we set $U = 1$ eV.

The model is analyzed with the use of a numerical renormalization group (NRG) method. We introduce a cut-off Λ for the logarithmic discretization of the conduction band. Due to the limitation of computer resources, we keep M low-energy states. Here we use $\Lambda = 8$ and $M = 5,000$. In the NRG calculation, the temperature T is defined as $T = D\Lambda^{-(N-1)/2}$, where D is half the conduction band width, which was set as 1 eV, and N is the number of renormalization steps.

From the NRG calculations, we have found a residual entropy $S_{\rm imp}$ of $\log\phi$ with the golden ratio $\phi = (1+\sqrt{5})/2$ for the local Γ_5 triplet ground state. For the multi-channel Kondo effect, the analytic value of the residual entropy $S_{\rm imp}$ has been found to be given by [2]

$$S_{\rm imp} = \log \frac{\sin[(2S+1)\pi/(n_{\rm c}+2)]}{\sin[\pi/(n_{\rm c}+2)]}, \qquad (2)$$

where S denotes the local impurity spin and $n_{\rm c}$ indicates the number of channels. In the present case with $n_{\rm c} = 3$, we obtain $S_{\rm imp} = \log\phi$ for both the cases of $S = 1/2$ and 1. Thus, in any case, the residual entropy $\log\phi$ is considered to be characteristic of the three-channel Kondo effect, but the value of S is not determined only from the residual entropy.

To confirm the value of S, we hit upon an idea to explore a quantum critical point (QCP) between the three-channel Kondo and Fermi-liquid phases. The QCP between the three-channel Kondo and Fermi-liquid phases is expected to be characterized by the residual entropy of the four-channel Kondo effect. From eq. (2), we obtain $S_{\rm imp} = 0.5\log 3$ and $\log 2$ for $S = 1/2$ and 1, respectively, for $n_{\rm c} = 4$.

In Fig. 3(a), we show the f-electron entropies for $W = 10^{-3}$ and $V = 0.7$ between $x = 0.65$ and 0.7. For $x = 0.65$, we observe the three-channel Kondo phase, while for $x = 0.7$, the local singlet phase appears. At $x = 0.6849$, the entropy plateaus with a value between $0.5\log 3$ and $\log 2$, and it eventually exits the plateau at around $T \sim 10^{-10}$. We deduce this as the signal of the QCP between the three-channel Kondo and Fermi-liquid phases. Note that this behavior has also been observed around at $x = -0.64$.

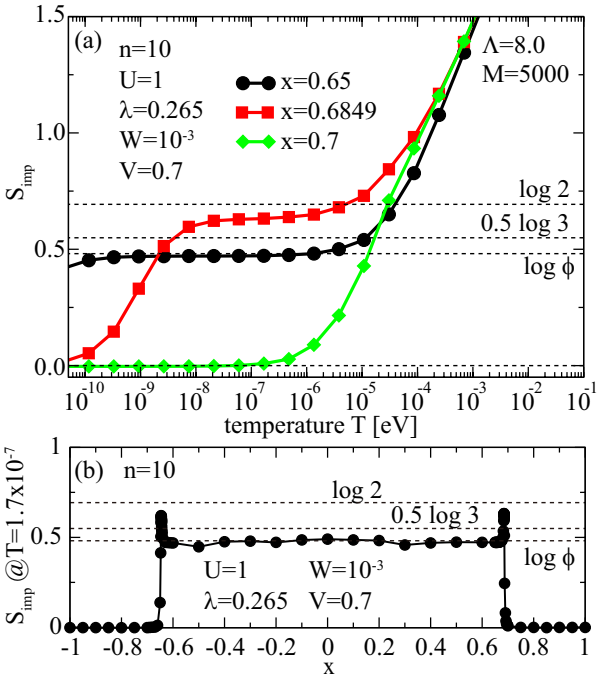

Figure 1: (a) Entropies vs. temperature for $x = 0.65$, 0.6849, and 0.7 with $W = 10^{-3}$ and $V = 0.7$. (b) Residual entropies at $T = 1.7\times 10^{-7}$ vs. x for $-1 \le x \le 1$.

In Fig. 3(b), we plot the value of the entropy at $T = 1.7\times 10^{-7}$ as a function of x for $-1 \le x \le 1$. We find sharp two peaks at around $x \approx -0.646$ and $x \approx 0.685$, and the peaks assume values between $0.5\log 3$ and $\log 2$. Since these values are apparently larger than $0.5\log 3$, we deduce that the peaks indicates the QCP characterized by the residual entropy of the four-channel Kondo effect with $S = 1$. This result is consistent with the local Γ_5 triplet ground state.

References

[1] T. Hotta, J. Phys. Soc. Jpn. **90**, 113701 (2021).

[2] I. Affleck and A. W. W. Ludwig, Nucl. Phys. B **360**, 641 (1991).

Magnetic field effect on excitonic phase in multi-orbital Hubbard model

Joji NASU
Department of Physics, Tohoku University
Sendai 980-8578

Excitonic insulators are insulating states where pairs of an electron in a conduction band and a hole in a valence band are condensed coherently. Although this state was proposed as a superconductivity analog about 50 years ago, recent discoveries of materials that could potentially exhibit excitonic insulators have renewed interest in studying this system. Among the candidates, cobalt oxides have received significant attention due to their multiple spin states, including low-spin, intermediate-spin, and high-spin states, which are affected by crystalline fields and Hund couplings. Recent research has suggested that excitonic condensation could occur through spontaneous hybridization between distinct spin states. The theoretical and experimental examinations of cobalt oxides in this perspective has revealed the emergence of a magnetic-field-induced excitonic phase and spin-splitting. The simplified two-orbital Hubbard model has been used in these studies to consider low-spin and high-spin states [1, 2, 3].

In this project, we have investigated magnetic field effects on the multi-orbital Hubbard model with the expressive ability of the three spin states, including the intermediate-spin state. We have derived a low-energy effective model and performed mean-field calculations, but due to the complexity of the model, finding solutions is computationally expensive. To reduce computation time, we have utilized the technique of parallel computation. Our findings show that increasing the applied magnetic field results in the appearance of two excitonic phases [4]. The low-field phase is not accompanied by spin-state alignments, while the excitonic phase appearing higher field is associated with a spin-state order and interpreted as a supersolid in terms of excitonic condensation. The magnetization curve should display signatures of these phases, which is consistent with a recent experiment measuring volume change up to 600T [4].

References

[1] T. Tatsuno, E. Mizoguchi, J. Nasu, M. Naka, S. Ishihara: J. Phys. Soc. Jpn. **85** (2016) 083706.

[2] J. Nasu, M. Naka, S. Ishihara: Phys. Rev. B **102** (2020) 045143.

[3] J. Nasu and M. Naka: Phys. Rev. B **103** (2021) L121104.

[4] A. Ikeda, Y. H. Matsuda, K. Sato, Y. Ishii, H. Sawabe, D. Nakamura, S. Takeyama, and J. Nasu: Nat. Commun. **14** (2023) 1744.

Correlation-induced phenomena in Kondo lattice systems

Robert PETERS

Department of Physics,

Kyoto University, Kyoto, 606-8502

Kondo insulators are strongly correlated insulators where the resistivity becomes large at low temperatures due to a gap in the single-particle spectrum [1]. Recently, quantum oscillations in strong magnetic fields have been observed in these materials while insulating. Furthermore, specific heat and thermal transport measurements on YbB_{12} and $YbIr_3Si_7$ have revealed low-lying excitations in these Kondo insulators that can transport heat but no electric current [2,3]. Thus, it has been argued that there are itinerant charge-neutral excitations that are responsible for thermal transport and lead to observable quantum oscillations in strong magnetic fields. However, a conclusion to these recent experiments is not yet found.

Using variational matrix product states, we analyzed the finite temperature behavior of a half-filled periodic Anderson model in one dimension, a prototypical model of a Kondo insulator. In our calculations [4], we confirmed the existence of energetically low-lying spin excitations [1] in this model and studied their energy-momentum dispersion and temperature dependence. We demonstrated that charge-charge correlations at the Fermi energy exhibit a different temperature dependence than spin-spin correlations. While energetically low-lying spin excitations emerge approximately at the Kondo temperature, which exponentially depends on the interaction strength, charge correlations vanish already at high temperatures.

Furthermore, we analyzed the charge and thermal conductivities at finite temperatures by calculating the time-dependent current-current correlation functions. While both charge and thermal conductivities can be fitted for all interaction strengths by gapped systems with a renormalized band gap, the gap in the system describing the thermal conductivity is generally smaller than the system describing the charge conductivity. Furthermore, the maximum of the charge conductivity over the temperature decreases monotonically with increasing interaction strength. On the other hand, the maximum of the thermal conductivity generally lies at smaller temperatures than the maximum of the charge conductivity and follows a nonmonotonic behavior , see Fig. 1. We thus found that charge and thermal conductivities are affected very differently by correlations and show a different temperature behavior.

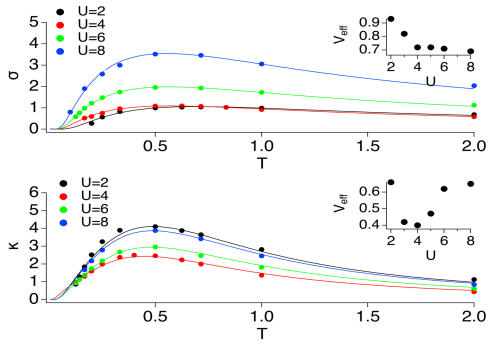

Figure 1: Charge conductivity and thermal conductivity for different interaction strengths. The insets show the effective gap in both conductivities.

In another work [5], we introduced a generalized quantum metric(GQM) on the Brillouin zone for correlated electron systems. This quantum metric is based on the optical conductivity that is written by single-particle Green's functions. We analytically proved that this definition is equivalent to the existing definition of the quantum metric in noninteracting systems and that it is positive semi-definite as necessary for a metric. Furthermore, we pointed out the relationship between the GQM and the Chern number in interacting systems. We then numerically confirmed these properties of the GQM in the Qi-Wu-Zhang model with and without interaction.

References

[1] H. Tsunetsugu, M. Sigrist, and K. Ueda
Rev. Mod. Phys. **69**, 809 (1997)

[2] Y. Sato, Z. Xiang, Y. Kasahara, T. Taniguchi, S. Kasahara, L. Chen, T. Asaba, C. Tinsman, H. Murayama, O. Tanaka, Y. Mizukami, T. Shibauchi, F. Iga, J. Singleton, Lu Li, and Y. Matsuda
Nature Physics **15**, 954 (2019)

[3] Y Sato, S Suetsugu, T Tominaga, Y Kasahara, S Kasahara, T Kobayashi, Shunsaku Kitagawa, K Ishida, R Peters, T Shibauchi, AH Nevidomskyy, L Qian, E Morosan, Y Matsuda, Nature comm. **13**, 394 (2022)

[4] R Peters and R Rausch, submitted to SciPost Physics

[5] T. Kashihara, Y. Michishita, and R. Peters
Phys. Rev. B **107**, 125116 (2023)

Electronic Structures of Nickel Dithiolene Complex-based Ambipolar Semiconductors

Tomoko FUJINO

Institute for Solid State Physics,

The University of Tokyo, Kashiwa-no-ha, Kashiwa, Chiba 277-8581

Air-stable single-component ambipolar organic semiconductors that conduct both holes and electrons are highly desired, but have been rarely realized. We synthesized neutral nickel bis(dithiolene) complexes (Fig. 1) that fulfill the stringent electronic requirements (i.e., shallow HOMO levels and deep LUMO levels) for air-stable ambipolar semiconductors [1]. The planar structures facilitated dense packing with effective intermolecular interactions. Remarkably, changing the methoxy substituents to ethoxy or propoxy groups led to a dramatic change in the packing mode from one-dimensional to herringbone-like, while maintaining effective intermolecular interactions, supported by the first-principles band calculation (OpenMX software). They are readily solution-processible to form active layers with well-defined and well-ordered structures in field-effect transistors. Devices based on these compounds exhibited efficient ambipolar characteristics, even after several months of exposure to air, whose carrier mobility are the top-class performances

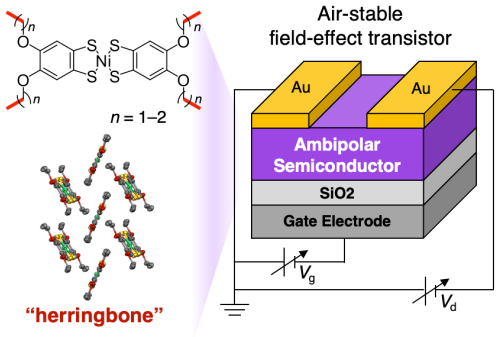

Fig. 1: Nickel dithiolene-based ambipolar semiconductors.

achieved for a single-component ambipolar semiconductor material driven in air.

References

[1] M. Ito, T. Fujino*, L. Zhang, S. Yokomori, T. Higashino, R. Makiura, K. J. Takeno, T. Ozaki, H. Mori*, J. Am. Chem. Soc. **145**, 2127 (2023), *Supplementary Cover*.

[2]. R. Kameyama, T. Fujino*, S. Dekura, S. Imajo, T. Miyamoto, H. Okamoto, H. Mori*, J. Mater. Chem. C **10**, 7531 (2022).

Inhomogeneous ground state due to kinetic energy effect in correlated electron systems

Takashi YANAGISAWA
National Institute of Advanced Industrial Science and Technology (AIST)
1-1-1 Umezono, Tsukuba 305-8568

1 Introduction

Our research is based on the optimized variational Monte Carlo method[1]. We use the optimized wave function improved by off-diagonal exponential operators such as $e^{-\lambda K}$ and $e^{-\alpha D}$ (K and D are the kinetic operator and the double occupancy operator, respectively), and the Gutzwiller-Jastrow wave function where the doublon-holon correlation is taken into account. We have investigated the ground-state phase diagram of the two-dimensional Hubbard model and the two-dimensional d-p model.

We performed parallel computation in Monte Carlo calculations. In order to reduce statistical errors, we carried out ~ 500 parallel calculations. Parallel computing is very important to reduce Monte Carlo statistical errors.

The many-body wave function is written in the form $\psi^{(1)} = \exp(-\lambda K)P_G\psi_0$, where K denotes the kinetic energy part (non-interacting part) of the Hamiltonian and $P_G = P_G(g)$ is the Gutzwiller operator to control the double occupancy with the variational parameter g. ψ_0 indicates a trial wave function which is usually taken as the Fermi sea, the BCS wave function or the state with some magnetic (or charge) orders. We can improve the wave function systematically by multiplying by operators P_G and $e^{-\lambda K}$ repeatedly. We can consider $\psi^{(2)} = \exp(-\lambda' K)P_G(g')\psi^{(1)}$ for different variational parameters λ' and g'. This wave function is a very good many-body wave function because the ground-state energy is lowered greatly and the ground-state energy is lower than those that are evaluated by any other wave functions. We also employ the Jastrow-type wave function which is written as $\psi_J = P_G P_Q P_J \psi_0$ where P_J indicates a nearest-neighbor number correlation operator and P_Q controls the nearest-neighbor doublon-holon correlation.

2 Ferromagnetic diagonal striped states in the Hubbard model

We have performed a variational Monte Carlo simulation to study the ground state of the two-dimensional Hubbard model on a square lattice. The energy gain of possible inhomogeneous electron states are computed as a function of U in the case where the hole density is $\delta = 1/8$ and next nearest-neighbor transfer $t'/t = -0.30$. The wave function is written as

$$\psi_{stripe} = P_{N_e} P_G P_J P_{DH} \psi_{MF}, \qquad (1)$$

where ψ_{MF} is the eigenstate of the following Hamiltonian

$$H_{MF} = -\sum_{ij\sigma} t_{ij} c^{\dagger}_{i\sigma} c_{j\sigma} + \frac{U}{2} \sum_{i\sigma} (\rho_i - \mathrm{sgn}(\sigma) m_i) n_{i\sigma}, \qquad (2)$$

with $\rho_i = \rho \cos(\mathbf{q}\cdot(\mathbf{r}_i - \mathbf{r}_0))$ and $m_i = m \sin(\mathbf{Q}\cdot(\mathbf{r}_i - \mathbf{r}_0))$. ρ and m are variational operators. Two incommensurate wave vectors $\mathbf{q}$ and $\mathbf{Q}$ characterize the charge and spin configurations, respectively. We set $\mathbf{q} = 2\mathbf{Q}$. $\mathbf{r}_0$ denotes the position of the domain boundary. P_{N_e} is the projection operator that extracts only the components with a fixed total number of electrons N_e. $P_{DH} = P_Q$ is the doublon-holon operator given by $P_{DH} = \prod_i (1 - (1-\eta)\prod_\tau d_i(1 - e_{i+\tau}))$ where $0 \le \eta 1$, $d_i = n_{i\uparrow} n_{i\downarrow}$, $e_i = (1 - n_{i\uparrow})(1 - n_{i\downarrow})$, and τ runs over all nearest-neighbor sites.

In Fig. 1, the energy difference per site between the normal and stripe states, $\Delta E = (E_{normal} - E_{stripe})/N_s$, of various stripe states at 1/8 doping, is shown as a function of U. The calculations were carried out on a 16×16 lattice. The results show that FM stripe states (open symbols) are more stable than AF stripe states (filled symbols) for $U/t \geq 16$.

The bond-centered ferromagnetic diagonal stripe state is stabilized in the strong coupling region with $U/t \geq 16$; this is due to the gain of both kinetic energy and on-site Coulomb interaction energy. The kinetic energy gain originates from the holon moving over the ferromagnetic domain and the gain of kinetic-exchange-interaction energy at the antiferromagnetic domain wall. For large U, the gain in the kinetic energy due to the transfer of holes on the ferromagnetic domain and that of the on-site Coulomb interaction energy exceed the loss of the kinetic exchange interaction energy, which leads to form an incommensurate electron state with the ferromagnetic domain.

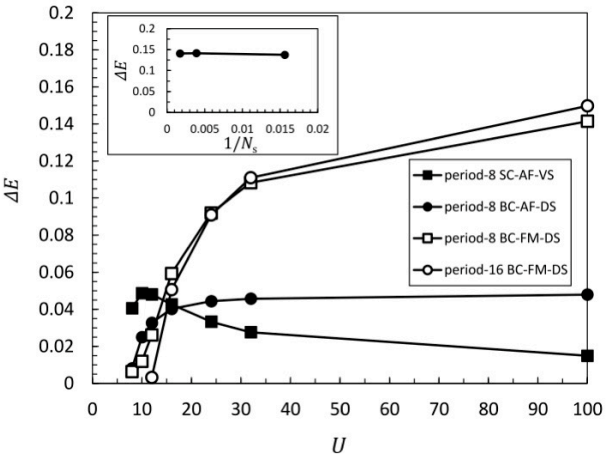

Figure 1: Optimized energy difference per site between the normal and striped states $\Delta E = (E_{normal} - E_{stripe})/N_s$ as a function of U. The data are from 16×16 lattices where electron number $N_e = 224$ (1/8 hole doping) and $t' = -0.30$. Filled squares indicate the period-8 bond-centered AF diagonal stripe state (8-period BC-FN-DS). Open squares (circles) denote the bond-centered FM diagonal stripe state (BC-FM-DS) with period-8 (period-16). Inset figure shows the system size dependence of the optimized energy difference per site for the period-8 BC-F-DS state with $U = 100$ at 1/8 hole doping. The error bars are smaller than the size of symbols.

3 Summary

We examined the ground state of the two-dimensional Hubbard model by using an advanced variational Monte Carlo method. In the strong coupling region where U is large, the kinetic energy gain is important in determining the ground state. In fact, the kinetic energy gain stabilizes superconducting state for the optimized BCS wave functions[3]. The kinetic term also plays an important role in striped states and the diagonal stripe becomes stable in this region due to the kinetic energy effect.

References

[1] T. Yanagisawa et al., J. Phys. Soc. Jpn. 67, 3867 (1998).
T. Yanagisawa, Phys. Rev. B75, 224503 (2007) (arXiv: 0707.1929).

[2] T. Yanagisawa, J. Phys. Soc. Jpn. 85, 114707 (2016).
T. Yanagisawa, J. Phys. Soc. Jpn. 88, 054702 (2019).
T. Yanagisawa, Condensed Matter 4, 57 (2019).

[3] T. Yanagisawa, Phys. Lett. A403, 127382 (2021).
T. Yanagisawa et al., EPL 134, 27004 (2021).

[4] M. Miyazaki, T. Yanagisawa, Phys. Lett. A448, 128276 (2022).

Unified description of cuprate high-temperature superconductors using multiband models

Hiroshi WATANABE
Research Organization of Science and Technology, Ritsumeikan University
1-1-1 Noji-Higashi, Kusatsu-shi, Shiga 525-8577

Understanding the various competing phases in cuprate high-temperature superconductors is a long-standing challenging problem. Although we have not yet reached a unified understanding of their properties, recent studies have shown that orbital degrees of freedom, both Cu e_g and O p orbitals, are key ingredient. Here we investigate the four-band *d-p* model that explicitly includes the $d_{x^2-y^2}$, d_{z^2}, p_x, and p_y orbitals [1, 2]. We construct the tight-binding energy bands for La_2CuO_4 and $HgBa_2CuO_4$ systems based on the first-principles calculation and examine the effect of Coulomb interactions with the variational Monte Carlo (VMC) method. The Gutzwiller-Jastrow type wave function is used for the VMC trial wave function. The system size for the calculation is N=24×24=576 unit cells (and thus 576×4=2304 orbitals in total) and the computation has been done mainly with the system B of the ISSP Supercomputer Center. We have compared the variational energies of various competing phases including superconductivity, ferro- and antiferromagnetic phases, and stripe phases with different periodicities to determine the ground state phase diagram for the hole doping rate x. We have also calculated physical quantities such as superconducting correlation functions, charge- and spin correlation functions, and local magnetic moments.

In Fig. 1, we show the hole density of the d_{z^2} orbital $n_{d_{z^2}}$ as a function of x for several values of Hund's coupling J/U_d at U_d/t_1=8, along with the superconducting correlation function P^{dd}. In La_2CuO_4, $n_{d_{z^2}}$ increases with x and is strongly enhanced by the Hund's coupling. This is because the system tends to increase $n_{d_{z^2}}$ to obtain the energy gain from the Hund's coupling. Since $n_{d_{z^2}}$ works destructively for superconductivity due to its localized character [1, 2], P^{dd} is suppressed by the Hund's coupling. On the other hand, in $HgBa_2CuO_4$, such an increase of $n_{d_{z^2}}$ and a suppression of P_{dd} are not so pronounced even for relatively large Hund's coupling. It results from the lower site energy $\varepsilon_{d_{z^2}}$ in the $HgBa_2CuO_4$ system that makes the d_{z^2} orbital almost inactive. The difference between two systems are well described in our four-band *d-p* model.

References

[1] H. Watanabe et al., Phys. Rev. Research **3**, 033157 (2021).

[2] H. Watanabe et al., J. Phys.: Condens. Matter **35**, 195601 (2023).

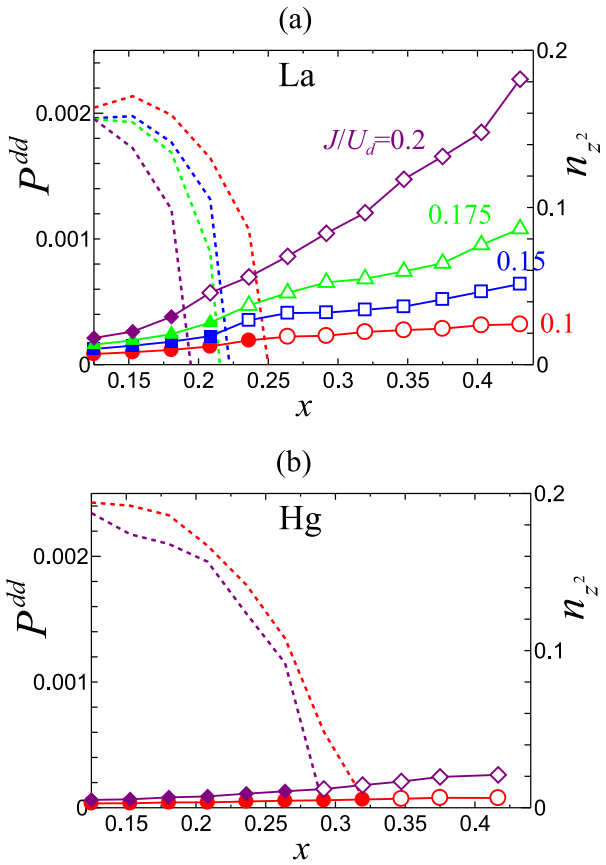

Figure 1: The hole doping rate x dependence of the hole density of the d_{z^2} orbital $n_{d_{z^2}}$ (solid lines with symbols) and superconducting correlation function P^{dd} (dotted lines) for (a) La_2CuO_4 and (b) $HgBa_2CuO_4$, respectively [2]. Solid (open) symbols correspond to the superconducting (paramagnetic) phase.

Gap opening mechanism for organic Dirac electron systems α-(BEDT-TTF)$_2$I$_3$ and α-(BEDT-TSeF)$_2$I$_3$

Akito Kobayashi[a], Daigo Ohki[a], Kazuyoshi Yoshimi[b] and Takahiro Misawa[b]
[a]*Department of Physics, Nagoya University, Nagoya 464-8602*
[b]Institute for Solid State Physics, University of Tokyo, Chiba 277-8581, Japan

In the Dirac electron system of organic conductors, phase transitions due to spontaneous symmetry breaking due to electron-electron interactions have been observed, and this has attracted interest as a research target for correlated Dirac electron systems. In α-(BEDT-TTF)$_2$I$_3$, it has been reported that the horizontal stripe charge order with inversion symmetry breaking induces a gap for massless Dirac electrons [1]. A related compound α-(BEDT-TSeF)$_2$I$_3$, on the other hand, has a distinctly different insulating state from α-(BEDT-TTF)$_2$I$_3$2 [2]. The gap opening mechanism has not yet been fully clarified.

To determine the origin of the differences in the gap opening mechanisms in α-(BEDT-TTF)$_2$I$_3$ and α-(BEDT-TSeF)$_2$I$_3$, we derive ab initio low-energy effective Hamiltonians and solve this using the many-variable variational Monte Carlo method (mVMC) [3]. It is found that an insulating state with the horizontal stripe charge order appears in α-(BEDT-TTF)$_2$I$_3$, which is consistent with experiments and previous studies as shown in Fig. 1(a). However, in α-(BEDT-TSeF)$_2$I$_3$, we find that an insulating state without any explicit symmetry breaking is realized. Because of the frustration in the inter-chain magnetic interactions, a dimensional reduction of the spin correlations occurs. As a result, one-dimensional spin correlations develop in α-(BEDT-TSeF)$_2$I$_3$ as shown in Fig. 1(b). This result suggests that the one-dimensional spin correlation induces the gap in α-(BEDT-TSeF)$_2$I$_3$, as in the one-dimensional Hubbard model [4]. Thus we found that α-(BEDT-TSeF)$_2$I$_3$ hosts massive Dirac electrons without symmetry breaking via dimensional reduction [5].

References

[1] H. Seo, J. Phys. Soc. Jpn. **69**, 805 (2000).

[2] S. Kitou et al., Phys. Rev. B **103**, 035135 (2021).

[3] T. Misawa et al., Phys. Commun. **235**, 447 (2019).

[4] E. H. Lieb and F. Y. Wu, Phys. Rev. Lett. **20**, 1445 (1968).

[5] D. Ohki et al., Phys. Rev. B **107**, L041108 (2023)

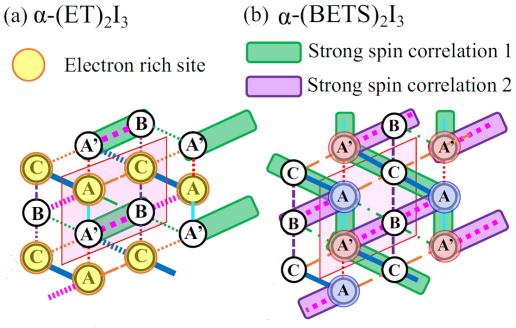

Figure 1: Schematic diagrams of α-type organic conductors for (a) α-(BEDT-TTF)$_2$I$_3$ and (b) α-(BEDT-TSeF)$_2$I$_3$.

Theoretical study of thermoelectric properties in Heusler compounds: A weak-coupling approach

Kazutaka NISHIGUCHI
Graduate School of System Informatics, Kobe University
Rokkodai-Cho, Nada-Ku, Kobe 657-8501

Heusler compound Fe_2VAl

Heusler compound Fe_2VAl is a promising thermoelectric material, which exhibits large power factor $P = \sigma S^2$ with σ and S being the electrical conductivity and Seebeck coefficient, respectively. On the other hand, the thermal the dimensionless figure of merit $ZT = \sigma S^2 T/\kappa$ is not so large yet reflecting its large thermal conductivity κ. Recently, it is experimentally observed in doped Fe_2VAl (i.e., $Fe_2V_{0.9}Cr_{0.1}Al_{0.9}Si_{0.1}$ and $Fe_{2.2}V_{0.8}Al_{1-y}Si_y$) as a weekly ferromagnetic material that ferromagnetic fluctuations enhance the thermoelectric properties such as S and P around the Curie temperature ($T_c = 285$ K). [1] It is not only a desirable property for practical use in realistic (room) temperatures, but also a fundamental and intriguing quantum phenomena where quantum fluctuations and thermoelectric effects are entangled by electron correlations.

Motivated above, we have studied electronic properties of Fe_2VAl using first-principles calculations based on the density functional theory (DFT) within the generalized gradient approximation (GGA). We performed DFT calculations with the Perdew–Burke–Ernzerhof (PBE) exchange-correlation functional and the projector augmented wave (PAW) method using The Vienna Ab Initio Simulation Package (VASP) [2] and Quantum ESPRESSO package. [3]

Using the maximally localized Wannier functions, we could construct a low-energy effective model from the first- principles bands around the Fermi level. The effective model is composed of the Fe-3d, V-3d, and Al-2sp3 Wannier orbitals, namely, 19 orbitals. The DFT b and structure and Wannier orbitals are shown in Fig. 1.

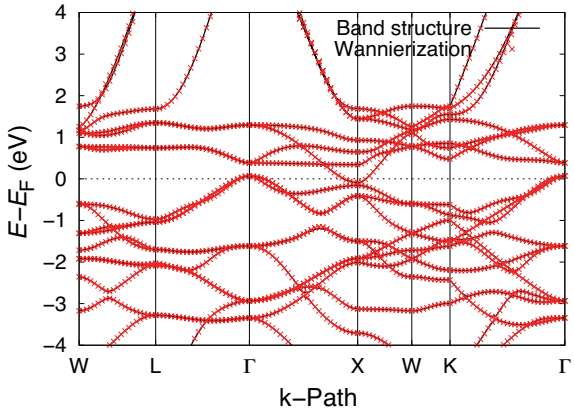

Figure 1: DFT band structure and Wannierization of Fe_2VAl.

Planar Defect in Layered Perovskite Photocatalyst $Y_2Ti_2O_5S_2$

Layered perovskite $Y_2Ti_2O_5S_2$ (YTOS) is a strong candidate for semiconductor photocatalysts suitable for overall water splitting under visible light. On the other hand, structural defects during synthesis should be controlled to improve photocatalytic performance similar to other photocatalysts [5]. Very recently, transmission electron microscopy (TEM) have revealed extremely large planar defects com-

posed of S–Mg–S layers in YTOS synthesized using the flux method.

We investigated the planar defect structure and electronic structure using first-principles calculations based on the density functional theory (DFT) [6]. The DFT calculations were performed within the PBE+U functional using PAW method, as implemented in VASP [2]. Here we set $U = 7.5$ eV for the $3d$ orbitals at the Ti sites to reproduce the experimental band gap, 1.9–2.0 eV [5].

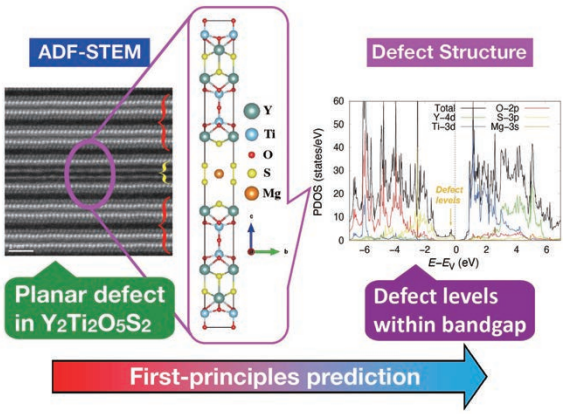

Figure 2: Planar defect in YTOS is investigated by electron microscopy and first-principles calculations.

We have microscopically determined the planar defect structure using the structural optimization, where a Mg atom is centered in the *ab*-square intersecting the defect S layers. The obtained defect structure is consistent with the ADF–STEM image. To understand the electronic structures, we have investigated the projected density of states (PDOS) and band structure, which shows that the defect bands appear within the original band gap. It is expected that such defect bands considerably increase the electron–hole recombination rate, enhancing the interband transitions of the defect valence and/or defect conduction bands via radiative or nonradiative transitions, which is an undesirable factor for the efficiency of the overall water splitting of YTOS. To consider the stability of the planar defect, we have finally evaluated the defect formation energy (E_f). The chemical potentials μ_i were determined by the phase diagram of the relevant compounds in the synthesis of YTOS. The evaluation of the formation energy suggests that E_f increases with decreasing μ_S and/or μ_Mg. Therefore, the optimum conditions for the S and Mg environments must be optimized for the synthesis of YTOS, which suppresses the formation of the planar defect.

References

[1] N. Tsujii, A. Nishide, J. Hayakawa, and T. Mori: Sci. Adv. **5**, eaat5935 (2019).

[2] G. Kresse *et. al.*: Phys. Rev. B **47**, 558 (1993); Phys. Rev. B **49**, 14251 (1994); Computational Materials Science **6** (1996) 15–50; Phys. Rev. B **54**, 11169 (1996).

[3] P. Giannozzi *et. al.*: J. Phys.: Condens. Matter **21**, 395502 (2009) ; J. Phys.: Condens. Matter **29**, 465901 (2017) ; J. Chem. Phys. **152**, 154105 (2020).

[4] I. Souza, N. Marzari, and D. Vanderbilt: Phys. Rev. B **65**, 035109 (2001) ; A. A. Mostofi *et. al.*: Comput. Phys. Commun. **178** (2008) 685–699; A. A. Mostofi *et. al.*: Comput. Phys. Commun. **185** (2014) 2309–2310; G. Pizzi *et. al.*: J. Phys.: Condens. Matter **32**, 165902 (2020).

[5] Q. Wang *et. al.*: Nat. Mater. **18**, 827 (2019) ; Z. Pan *et. al.*: Res. Chem. Intermed. **47**, 225 (2021).

[6] M. Nakabayashi, K. Nishiguchi, X. Liang, T. Hisatomi, T. Takata, T. Tsuchimochi, N. Shibata, K. Domen, and S. L. Tenno: J. Phys. Chem. C 2023, **127**, 7887–7893 (M.N. and K.N. contributed equally to this work).

Nonequilibrium dynamics induced by optical driving

Atsushi ONO
Department of Physics, Tohoku University,
Sendai 980-8578

The ultrafast dynamics of electrons in solids have been actively studied in recent years. For example, high-harmonic generation, which yields harmonics several tens of times higher than the incident light, has attracted interest as a phenomenon for generating broadband ultrashort pulses, while its mechanism involves nonperturbative and nonlinear processes, requiring accurate numerical calculations to understand such intriguing ultrafast phenomena.

This year, we focused mainly on the nonequilibrium dynamics of photocarriers excited by a resonant optical pulse and then driven by an optical electric-field pulse. We considered theoretical models of band insulators, Mott insulators, and charge-ordered insulators and calculated the real-time evolution using exact diagonalization and infinite time-evolving block decimation methods on the ISSP supercomputer system.

We found that in a band insulator, the optical driving pulse changes the relative velocity of photocarriers, resulting in carrier recombination and the generation of echoes of the excitation pulse. A detailed analysis revealed that the frequency of the echo pulses reflects the energy dispersion relation of the photocarriers. Furthermore, we performed numerical calculations for Mott insulators described by the Hubbard model and found that echo pulses can also be generated despite the breakdown of the single-electron picture, and their frequencies coincide with the energy of the doublon–holon pairs obtained from the Bethe ansatz, as shown in Fig. 1. We found that this echo phenomenon, termed an energy-band echo, can be observed in various insulators and reflects the dispersion relation of itinerant quasiparticles.

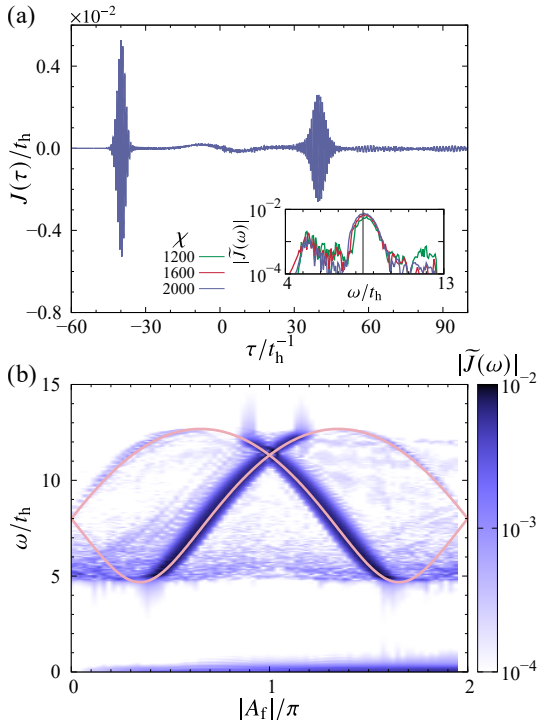

Figure 1: Echoes in a one-dimensional Mott insulator [1]. (a) Time profile of the electric current. The inset shows the Fourier spectrum. (b) Fourier spectral map of the electric current. The red curves show the dispersion relations of the doublon–holon pair. A_f is proportional to the amplitude of the optical driving pulse.

References

[1] S. Imai, A. Ono, and S. Ishihara, Phys. Rev. Research **4**, 043155 (2022).